Label-Free Detection of Morpholino-DNA Hybridization Using a Silicon Photonics Suspended Slab Micro-Ring Resonator

Soha Yousuf, Jongmin Kim, Ajymurat Orozaliev, Marcus S. Dahlem, Yong-Ak Song, and Jaime Viegas

***Abstract*—In this study, deoxyribonucleic acid (DNA) hybridization was demonstrated using a suspended silicon photonics micro-ring resonator with a 90 nm-thick slab and morpholino as the capture probe. Complementary DNA of various concentrations were tested achieving a surface sensitivity of 2.12 nm/nM, a detection limit of 250 pM, and an intrinsic detection limit of 36.9 pM. A bulk sensitivity of 98 nm/RIU and an intrinsic detection limit of 1.03×10^{-3} RIU was also measured upon exposure to isopropanol/deionized water solutions. With these characteristics, the suspended 90 nm slab ring sensor proved as a promising candidate for lab-on-a-chip bio-sensing applications.**

***Index Terms*—Morpholino-DNA hybridization, label-free, micro-ring resonator, bio-sensor.**

I. Introduction

DNA-BASED diagnostics has been developing rapidly over the years due to its extensive applications in disease diagnosis [1], detection of clinical illnesses such as cancer [2], [3], environmental monitoring [4], and food science [5]. Particularly in the healthcare industry, accurate detection of genetic and viral diseases rely on the provision of precise and cost-effective results. Therefore, the development of inexpensive and highly sensitive devices that have a small footprint has been the subject of intense research efforts. Now more than ever, such a need is urgently pressing with the imminent health threat that viruses such as SARS-CoV-2 have challenged the medical field with.

The specificity and sensitivity of hybridization are mainly influenced by the binding efficiency between target DNA and the capture probe. Morpholino (MO) probes are synthetic nucleic acid analogs that have the sugar phosphate backbone of a natural nucleic acid replaced with alternating morpholine rings connected by phosphorodiamidate groups, resulting in a non-ionic backbone [6]. Compared to other uncharged DNA analogs such as peptide nucleic acids (PNA), morpholinos have exhibited greater flexibility to oligomer length to bind to longer DNA targets. Their promise as enhanced capture probes comes from their unique properties including - great water solubility, stability, high hybridization efficiency, and specificity. In comparison to DNA probes that hybridize at high ionic strengths (0.1 - 1 M), morpholinos allow for DNA detection at much lower ionic strengths (down to 10 mM), due to the probe's backbone charge neutrality which exhibits low electrostatic hindrance [7].

By far, the largest impact of morpholinos in diagnostic research has been achieved through the improvisation of transductional means, especially those based on electrostatic and conductivity principles. Label-free hybridization between immobilized MO probes and DNA targets have been detected by monitoring interfacial capacitance fluctuations on gold supports [8], where signals using uncharged MO probes were of higher magnitudes, compared to DNA probes. In [6], an electrochemical sensor employed morpholino probes as a capture probe and a cationic redox polymer as a signal generator in order to detect hybridized DNA. In another approach, zirconium ions were used to fluorescently label hybridized DNA to morpholino films employing the phosphate-zirconium-carboxylate coordination reaction. The method exhibited a linear behavior of the fluorescent readout for various DNA concentrations (1 pM to 1 nM) [9]. Other nanostructures that have exploited the benefits of morpholino probes include silicon nanowires, such as reported by Zhang *et al.* [10]. The hybridization of DNA was detected from the fluctuation in nanowire conductance at a sensitivity of 100 fM.

Despite the great promise that morpholino exhibits as a capture probe, it faces some restrictions similar to those of conventional methods. These include long hybridization time and low hybridization sensitivity, especially for low target analyte concentrations. Both these challenges are normally tackled using amplification techniques prior to hybridization, such as the polymerase chain reaction (PCR) which is not feasible in

Manuscript received April 6, 2021; revised July 9, 2021; accepted July 15, 2021. Date of publication July 21, 2021; date of current version September 9, 2021. This work was supported in parts by the Mubadala Development Company, Abu Dhabi, Economic Development Board, Singapore, and GlobalFoundries, Singapore under the framework of the 'Twinlab' project, with participation of A*STAR Institute of Microelectronics, Singapore, and in part by the Khalifa University under Grants CIRA-2018-110 and CRPA-2020-019. *(Corresponding author: Soha Yousuf.)*

Soha Yousuf was with the Department of Electrical Engineering and Computer Science, Khalifa University of Science and Technology, Sas Al Nakhl Campus, Abu Dhabi 127788, UAE. He is currently with the Division of Science, New York University Abu Dhabi, Abu Dhabi 129188, UAE (e-mail: sohaekrima@gmail.com).

Jongmin Kim, Ajymurat Orozaliev, and Yong-Ak Song are with the Division of Engineering, New York University Abu Dhabi, Abu Dhabi 129188, UAE (e-mail: jk181@nyu.edu; ajymurat.orozaliev@nyu.edu; rafael.song@nyu.edu).

Marcus S. Dahlem is with the Interuniversity Microelectronics Center (IMEC), 3001 Leuven, Belgium, and also with the Department of Electrical Engineering and Computer Science, Khalifa University of Science Abu Dhabi 127788, UAE (e-mail: mdahlem@alum.mit.edu).

Jaime Viegas is with the Department of Electrical Engineering and Computer Science, Khalifa University of Science and Technology- Sas Al Nakhl Campus, Abu Dhabi 127788, UAE (e-mail: jaime.viegas@ku.ac.ae).

This article has supplementary material available at https://doi.org/10.1109/JPHOT.2021.3098680, provided by the authors.

Digital Object Identifier 10.1109/JPHOT.2021.3098680

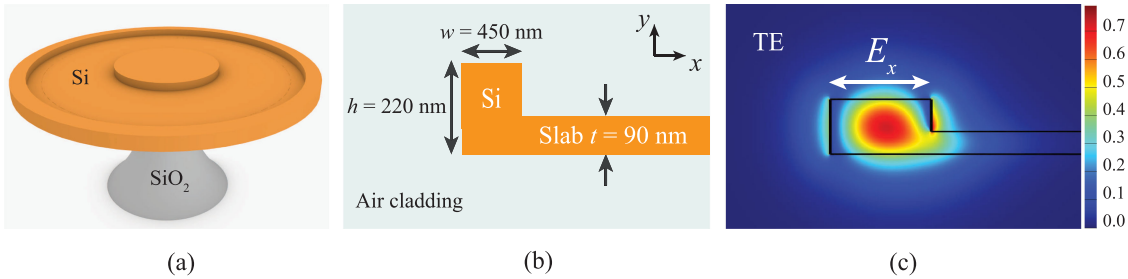

Fig. 1. Design of a suspended 90 nm slab micro-ring resonator; (a) Schematic of the structure; (b) Illustration of the transverse cross-section of the structure; (c) Simulated optical E_x field for the suspended portion of the ring with TE mode launched ($h = 220$ nm, $w = 450$ nm, and slab $t = 90$ nm).

clinical diagnostic applications [11]. Therefore, a direct, rapid, and simple detection scheme that reliably detects the target analyte at high sensitivity has yet to be explored.

In this regard, optical bio-sensing devices such as silicon photonic sensors have attracted interest due to their high sensitivities and label-free detection approaches, becoming one of the most commonly used for nucleic acid detection [12]. They yield great promise owing to their low fabrication cost in high volumes with CMOS-compatible processes, sensitivity to adsorbed biomolecular layers at their surface, and their highly compact footprint.

In particular, resonant cavities such as micro-ring resonators [13], [14], whispering gallery mode resonators [15], disks [16], droplet resonators [17], [18], grated rings [19], and photonic crystals [20] are regarded as attractive devices for bio-sensing applications, and have been explored experimentally extensively, as well as theoretically, through simulations [21], [22]. The surface binding causes a change in the effective index of the propagating mode that is translated into a shift in the resonant wavelength position [23]. Target analytes bound on the surface of these waveguides are sampled hundreds times over because of the re-circulation of light within the micro-cavity when in resonance [24]. This feature offers a great advantage to reduce the device size by orders of magnitude without sacrificing the interaction length owing to high Q-factor resonances, which is particularly crucial when detecting low analyte concentrations [25]. However, despite the growing interest, deploying morpholino as a capture probe on resonant optical structures like micro-ring resonators has been limited.

In this work, morpholino-DNA hybridization has been demonstrated on a suspended 90 nm-thick slab micro-ring resonator that uses covalent bonding as the surface functionalization protocol to immobilize morpholino capture probes onto the ring's waveguide surface. The suspended structure improved sensor sensitivity by enhancing light-matter interaction between target biomolecules and the evanescent field of the resonant cavity. To the best of our knowledge, this bio-sensing experiment demonstrated the potential of utilizing morpholino as a DNA capture probe on a suspended photonic micro-ring resonator for the first time. A linear relationship was demonstrated between the resonant wavelength shifts and the target DNA concentrations. A bulk refractive index sensitivity was also reported for the device using varying concentrations of deionized (DI) water and isopropanol (IPA) solutions. On the whole, the suspended 90 nm slab micro-ring resonator addressed many of the MO-based shortcomings, and proved as a potential sensing platform for lab-on-a-chip applications.

II. Device Simulation and Analysis

The 90 nm-thick slab micro-ring resonator structure is illustrated in Fig. 1. The reason behind choosing a slab thickness of 90 nm was constrained to the thickness offered by the fabricating foundry. The design was previously proposed in [26] using a multimode core width to achieve a large Q factor. However, for interferometric structures such as micro-ring resonators, single mode waveguides are preferred for bio-sensors in order to curb ambiguous results [27], [28].

Therefore, in this work, a similar design to [26] was proposed, ensuring only the excitation of the fundamental mode at a wavelength of 1550 nm, for a designed waveguide core width of 450 nm. This feature would help cater towards increasing the ring's sensitivity to changes in the external medium due to less confinement of the mode in the silicon core. In addition, removing the top and bottom oxide layer yields a greater portion of the optical mode to interact with the surrounding medium which results in an increase in sensitivity. In this regard, by removing the buried oxide completely from under the ring using a timed isotropic etch, the micro-ring resonator is suspended, while permitting a portion of this oxide to remain under the central Si disk. This forms an oxide pedestal that mechanically supports the entire structure.

The functionalization layers and binding of a target analyte to an immobilized probe can increase the thickness of the resulting surface layer from a few - to several hundreds of nanometers [29]. Therefore, the surface sensitivity becomes an important figure of merit. In a micro-ring resonator, the surface sensitivity (S_s) assesses the resonant wavelength shift per change in refractive index, within the first few hundreds of nanometers of adlayer thickness above the waveguide surface [30], [31].

To quantify the thickness of the deposited layers on the surface of the sensor ring in relation to experimental results, a simple model can be used to simulate the behaviour. A uniform layer is placed surrounding all four sides of the waveguide with a constant refractive index, as illustrated in the schematic of Fig. 2. Realistically, the resonant wavelength shift for each layer deposition would correspond to the respective refractive index changes based on the molecular weight of the molecule. However, the

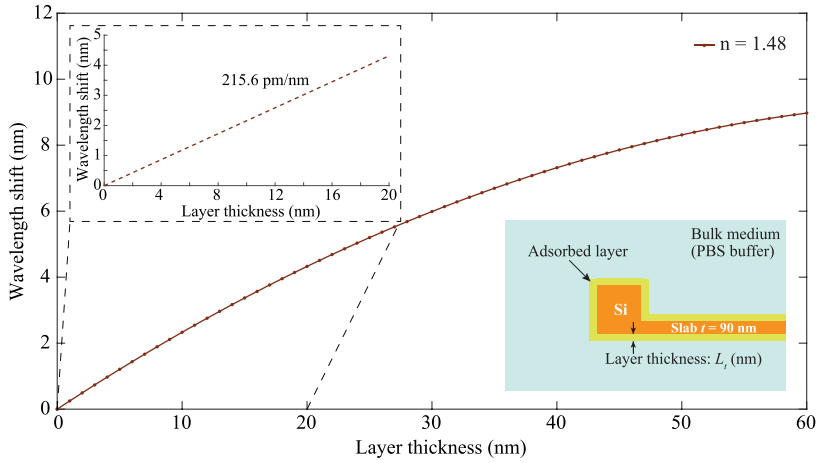

Fig. 2. Resonant wavelength shift as a function of biomolecule layer thickness for an adsorbed layer with refractive index ($n = 1.48$) on a 90 nm-thick slab waveguide cross-section of dimension (450×220 nm). The graph inset shows the simulated surface sensitivity.

majority of previous studies have simplified the model and conducted simulations by varying the surface layer thickness with a constant refractive index, to provide an understanding into the amount of adsorbed layers [30], [32], [33]. The resonant wavelength shift due to simulated deposited layers is calculated using (1) [32]:

$$\Delta\lambda = \frac{\Delta n_{\text{eff}} \times \lambda_0}{n_{\text{g}}}, \tag{1}$$

Where Δn_{eff}, λ_0, and n_g represent the change in the effective refractive index of the propagating mode due to the presence of a biomolecule layer, the initial resonant wavelength, and the group index, respectively. The effective index change, Δn_{eff} was simulated using Lumerical MODE solver where changes were assumed to be linear, starting from a bulk solution (no biomolecule layer) to an increased biomolecule layer thickness, until a densely packed monolayer was achieved. The corresponding resonant wavelength shift was then calculated using (1).

A mesh independency test was conducted to resolve the nanometer-size adsorbed biomolecule layer. A finer mesh was placed at the biomolecular region around the 90 nm slab micro-ring resonator, as demonstrated in Fig. S1 (a) and (b) in the supplementary material.

When the maximum mesh step was set at a value of 1 nm, the resulting effective refractive index at a simulated wavelength of 1.55 μm, was 2.4389. When the mesh step was decreased to 0.5 nm, the effective index of the slab ring was 2.4390. Therefore, a minimal difference of ~ 0.004 % exists, which can be considered as negligible. In addition, comparing Fig. S1 (a) and (b) with mesh step settings (1 nm and 0.5 nm), a biomolecular thickness of 1 nm is easily discernable with a maximum mesh step of 1 nm, which is the minimum layer thickness simulated. Therefore, a maximum mesh step of 1 nm was chosen for the mesh overlay on the biomolecular layer in order to save the computational time.

Adsorbed protein films are usually modeled with a refractive index between that of dry molecules and of the surrounding solution. The refractive index for adsorbed, hydrated proteins, has been confirmed to be between 1.48 - 1.50 [30], [33] which could be used to simulate for DNA molecules as well [32]. The surrounding aqueous solution for the hybridization of target DNA is phosphate buffer saline (PBS) whose refractive index was set to $n_{\text{pbs}} = 1.33$ at a wavelength of 1550 nm [33].

It was assumed that the refractive index of the layers that would mimic the surface functionalization layers and the target DNA would have a constant refractive index ($n = 1.48$), but with a changing effective thickness, given that surface coverage of adsorption is not 100%. As can be seen from the graph inset in Fig. 2, for layer thicknesses up to 20 nm, the sensor response was almost linear, and the thickness was far beyond that of experimentally detectable adsorbed layers. Thus, using this range of thickness, a fitted simulated surface sensitivity ($S_{\text{s}} = \Delta\lambda/\Delta t$) of 215.6 pm/nm was estimated for an adsorbed biomolecule layer with constant refractive index ($n = 1.48$).

III. Experimental Methods

A. Fabrication Process

The fabrication of the 90 nm slab micro-ring resonator was conducted by A*STAR Institute of Microelectronics-Singapore using a 248 nm optical lithography process.

The suspended resonator was fabricated on an SOI wafer which comprised of a 220 nm thick Si structure layer, 2 μm buried oxide layer and 725 μm Si substrate. A hard mask was used to etch the waveguide pattern on the structure layer to a depth of 130 nm. This formed a slab layer with a thickness of 90 nm. The Si layer was then patterned and etched using photoresist to define the outer edge of the ring having a height of 220 nm. The photoresist and hard mask were then stripped and etched off, respectively. Then, 2 μm thick SiO_2 was deposited to form the upper cladding, patterned and etched for subsequent deposition of 750 nm of aluminum as metal pads. A protective layer was deposited all over the device and patterned to create access to the metal pads and a window to the targeted micro-ring resonator. This window was used to etch the deposited and buried oxide layers using hydrofluoric acid, which resulted in a suspended silicon micro-ring resonator, with a portion of

TABLE I
MORPHOLINO PROBE AND SSDNA TARGET GENETIC SEQUENCES

Comments	Sequence
MO ssDNA probe	5' GTA GCT AAT GAT GTG GCA TCG GTT G 3'
Complementary ssDNA target	5' CAT CGA TTA CTA CAC CGT AGC CAA C 3'

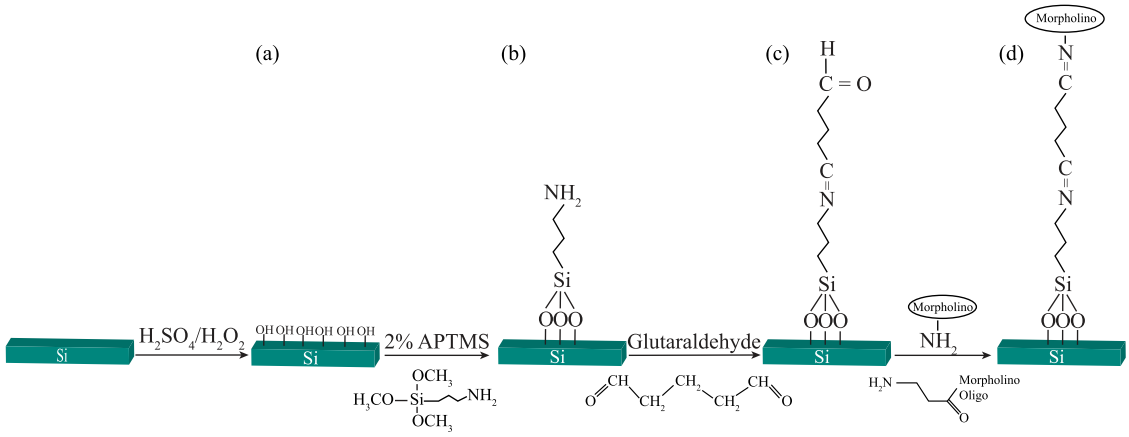

Fig. 3. Schematic of functionalizing Si surface with MO probe for DNA sensing; (a) Hydroxylation of Si with 3:1 H_2SO_4:H_2O_2 solution; (b) Salinization reaction between APTMS and the hydroxylated surface terminating it with NH_2 amine groups; (c) Cross-linking with glutaraldehyde; (d) Covalently immobilizing the 5'-NH_2 modified morpholino ssDNA probe ready for DNA hybridization. Details of the surface functionalization protocol can be found in the Supplementary Material.

the oxide remaining under the Si slab portion of the ring, to mechanically support the entire structure.

B. Measurement Setup

To characterize the fabricated 90 nm slab micro-ring resonator, an optical setup was used with a C/L-band tunable laser (Agilent 81600B Tunable Laser Source) as the input-light source covering the wavelength range (1460 nm-1640 nm). A MATLAB script was remotely accessed to sweep the laser wavelength for data acquisition. Polarized light (TE/TM mode) set through manual fiber polarization controllers was coupled to, and retrieved from the silicon chip under test. This was achieved using a pair of lens-tipped fibers with a focal spot size of 1.7 μm, with the return light detected by an optical power sensor (InGaAs Agilent 81636B detector). The output was imaged on a visible camera with a 20X microscope objective lens, and an infrared camera for visual observation of propagating light in the waveguides. The chip was stabilized on a custom aluminum chuck using vacuum. Along with the lensed fibers, the components were placed on a set of xyz translation stages using Thorlabs piezo controllers to allow for optimum edge-coupling to the silicon chip.

C. Surface Functionalization Protocol for MO-DNA Hybridization

For the experimental demonstration of label-free single stranded DNA (ssDNA) hybridization, the surface of the fabricated 90 nm slab micro-ring resonator was functionalized based on the covalent bonding method, to immobilize morpholino probes. This method is commonly known to provide good stability and high binding strength [34]. Details of the surface functionalization protocol can be found in the Supplementary Material.

For the MO-DNA hybridization experiments, we used a 25-mer length morpholino probe and a 25-mer length ssDNA complementary target whose sequences are shown in Table I. The entire process of the surface functionalization chemistry of the 90 nm slab micro-ring resonator surface is illustrated in Fig. 3.

IV. RESULTS AND DISCUSSION

The 90 nm-thick slab micro-ring resonator was fabricated by A*STAR Institute of Microelectronics-Singapore using a 248 nm optical lithography process as elaborated in Section III-A, with the targeted dimensions, as shown in Fig. 1 (b): outer Si ring with a thickness of 220 nm and a width of 450 nm, inner slab thickness of 90 nm, input and output waveguide widths of 450 nm, a coupling gap of 200 nm, and ring radii of 6 μm and 10 μm.

An SEM image of the fabricated 90 nm slab micro-ring resonator is shown in Fig. 4 (a). The magnified SEM image in Fig. 4 (b) illustrates the oxide cladding that has been etched from underneath the outer ring, suspending the structure. An oxide pedestal remains under the silicon disk portion of the ring resonator (not shown).

A. Bulk Refractive Index Sensitivity

Testing bulk refractive index changes is crucial to investigate, as solutions with different refractive indices contribute to the overall measurement result. In addition, in some diagnostic

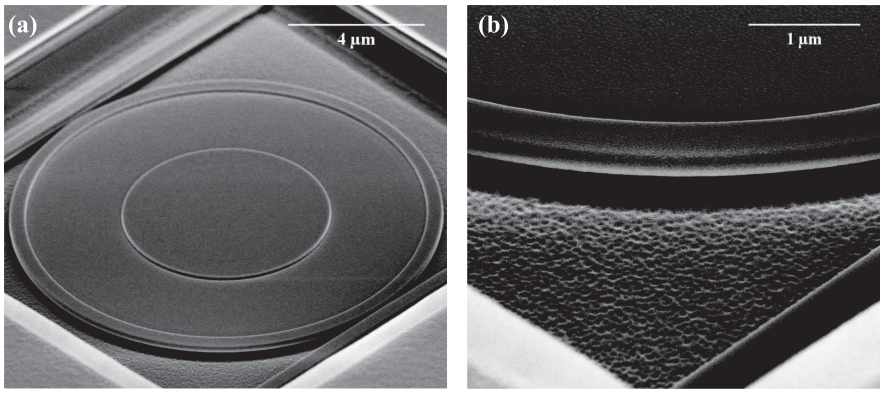

Fig. 4. A fabricated suspended 90 nm slab micro-ring resonator; (a) Scanning electron microscope image of the micro-ring resonator fabricated using deep UV lithography; (b) Zoom-in of the suspended ring with the oxide cladding etched from underneath the outer ring.

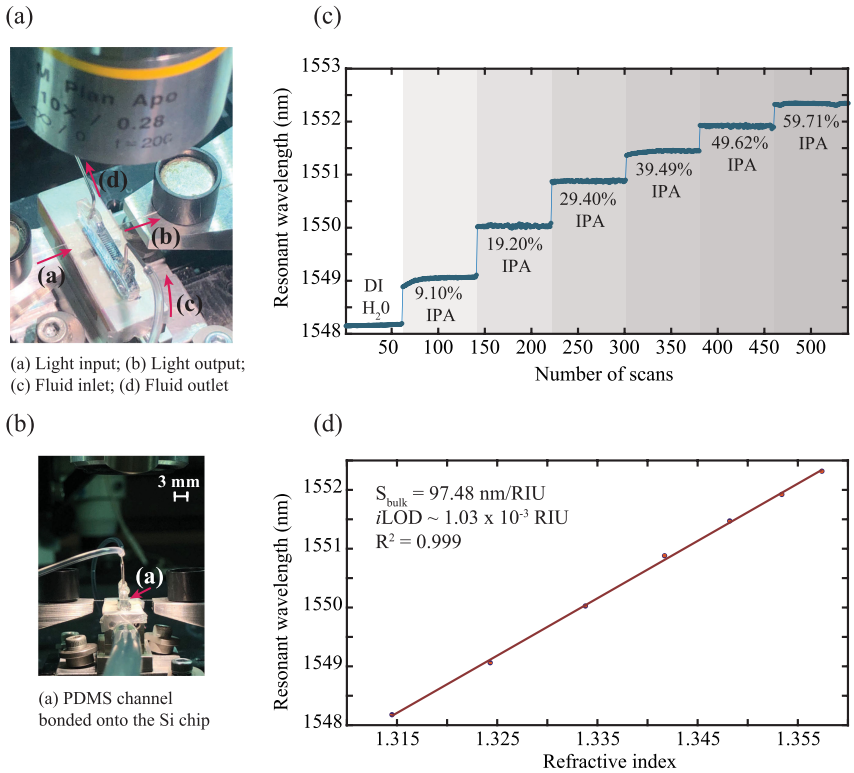

Fig. 5. Bulk sensitivity experiment using isopropanol/DI water concentrations; (a) Experimental setup showing a PDMS microfludic channel bonded onto the silicon chip; (b) Side view of the microfluidic channel bonded onto the silicon chip; (c) Resonant wavelength shifts of a 90 nm slab micro-ring resonator for different isopropanol/DI water concentrations; (d) Sensitivity plot for 9.1% - 59.71% IPA solutions with refractive indices (n = 1.3145 - 1.3574). A bulk refractive index sensitivity, S_{bulk} of 97.48 nm/RIU and an iLOD of 1.03×10^{-3} RIU was achieved.

applications, the concentration of the bulk solution is essential (e.g. glucose monitoring).

Liquids with varying refractive indices (different concentrations of isopropanol and deionized water) were flown across a 10 μm-radius 90 nm slab micro-ring resonator, with an FSR of about $\sim$ 9 nm. This was conducted using a plasma-bonded PDMS microfluidic channel on the surface of the silicon chip (Fig. 5 (a)), the details of which can be found in the Supplementary Material. Using syringes and a microfluidic pump, different liquids were flown at a constant flow rate of 5 μl/min. All measurements were scanned at a total number of $\sim$ 80 times, that was sufficient enough to ensure stability of the shifted resonant wavelength as a new solution was flown over the micro-ring resonator.

Fig. 5 (c) shows the resonant wavelength shift with increasing IPA concentration in the prepared solution. As a result, a linear shift of $S_{\mathrm{bulk}} = 97.48$ nm/RIU (bulk sensitivity) was obtained, as can be seen from Fig. 5 (d). The linear fit is represented with mean wavelength shift values and weighted standard deviation error bars. The variations were minimal, proving very high stability.

The temperature effect on the performance of the 90 nm slab micro-ring resonator was not accounted for experimentally. However, a MODE simulation was conducted to obtain

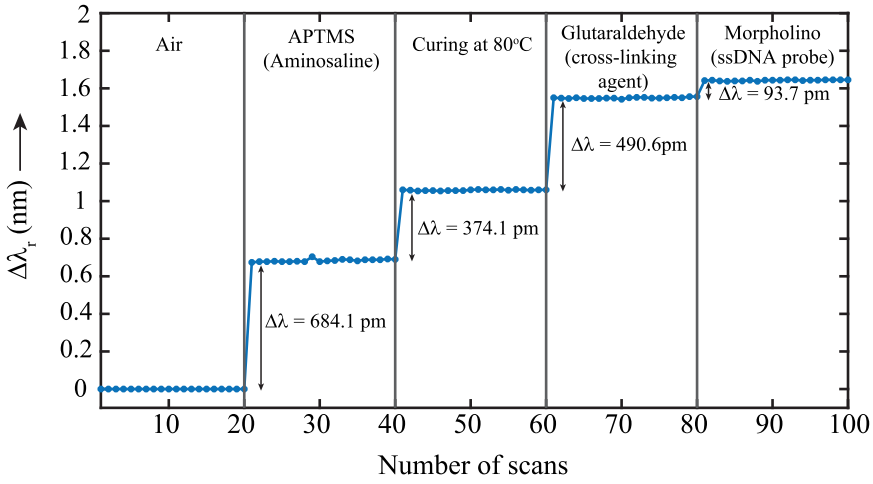

Fig. 6. Resonant wavelength shifts of the 90 nm slab micro-ring resonator sensor with respect to each surface functionalization step. Each resonant wavelength shift was with respect to the prior step.

an estimated temperature sensitivity, considering the thermo-optic coefficient (TOC) of the silicon layer and the aqueous cladding. Since water was the base of the DI water/IPA solution, it was set as the cladding. The TOC ($\partial n/\partial T$) for silicon was approximated to be $\sim 1.8 \times 10^{-4}$ / °C [35], and ($\partial n/\partial T$) $\sim -9.9 \times 10^{-5}$ / °C [36] for water, at 25 °C. According to Hale and Querry [37], the refractive index of water at T = 25 °C and 1550 nm wavelength is 1.318. Therefore, the refractive index of the cladding was set to 1.318, and the change in temperature was simulated by changing the refractive index according to the water's thermo-optic coefficient. In order to simulate a temperature from 20 °C to 30 °C, the refractive index was swept between 1.3185 and 1.3175, resulting in an estimated sensitivity of - 63.49 pm/ °C, as shown in Fig. S2 in the Supplementary material. The change in sign of sensitivity is due to the thermo-optic coefficient of water. As expected, the temperature's sensitivity of this sensor is much lower than its sensitivity to the refractive index, by about a 150-fold factor.

For a tracked resonant wavelength ($\lambda_{\rm res}$ = 1548.24 nm) whose Q factor was fitted to a value of 15 490, the achieved intrinsic limit of detection (iLOD) of the device was $\lambda_{\rm res}/(Q \times S_{\rm bulk}) = 1.03 \times 10^{-3}$ RIU. The low detection limit was comparable to values obtained in [19] and [38]. In addition, the detection limit and the bulk sensitivity showed a 2.5-fold enhancement in performance as compared to values obtained in [39].

Although the detection limit of our suspended micro-ring resonator is higher in comparison with reported ones, it has the advantage of being fabricated with the industrial standard microfabrication process using the 248 nm optical lithography process. Therefore, it is definitely industrially scalable and offers the opportunity for commercialization with standard mass microfabrication techniques.

For instance, the sensitivity of the subwavelength multibox waveguide reported in [19] was higher (579.5 nm/RIU) than ours. However, the iLOD was on the order of (10^{-3} RIU), due to the low Q factor (2600) measured in water. Furthermore, its fabrication required a multi-etch process EBL process, or the advanced 193 nm immersion lithography technology [19], which significantly complicated the fabrication process. The 220 nm thick TE mode ring resonator reported in [39] achieved an iLOD of 2.72×10^{-3} RIU, a sensitivity of 38 nm/RIU, and the dual polarization micro-ring resonator in [40] achieved a sensitivity of 104 nm/RIU for the TE mode, despite both resonators being fabricated with ebeam lithography. In comparisoin, using the standard 248 nm optical lithography microfabrication process, we obtained a (higher,similar) sensitivity at a comparable detection limit.

B. Label-Free Detection of MO-DNA Hybridization

To establish the DNA detection sensitivity of the micro-ring resonator with a radius of 6 μm (Q factor of 19 840, FSR of $\sim$16 nm) and inner slab thickness of 90 nm, resonant wavelength shifts were first recorded for each step of the protocol highlighted in Section III-C and described in the Supplementary Material.

Fig. 6 illustrates the resonant wavelength shifts with respect to each surface functionalization step. After piranha cleaning, the sample blue shifted the resonance (not shown), while the resonant wavelength red shifted after each molecular attachment step. The layering of biomolecules on the 90 nm slab ring surface increased the effective refractive index of the micro-ring resonator which influenced the resonant wavelength shift. A total wavelength shift of $\Delta\lambda_{\rm r}\tilde{}\sim 1.643$ nm occured between no monolayer in air, and a morpholino-functionalized monolayer. It should be noted that the surface functionalization and the subsequent hybridization of the target ssDNA to the immobilized MO probe was conducted in an open environment without a PDMS chip.

A series of varying concentrations of complementary ssDNA (0.25 nM, 0.5 nM, 0.75 nM, and 1 nM) in 0.1X PBS solution were tested. Hybridization of the DNA to the morpholino ssDNA probe showed linear wavelength shifts with the DNA concentrations, as shown in Fig. 7 (a). In Fig. 7 (b), each bar corresponds to the resonant wavelength shift after hybridization of morpholino to the target ssDNA concentration. Based on the experimental results, the sensitivity of the 90 nm slab micro-ring resonator

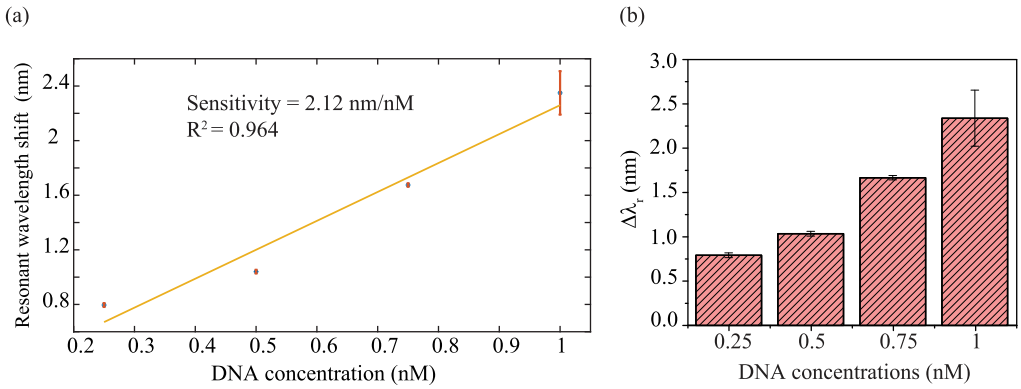

Fig. 7. MO – DNA hybridization results; (a) Plot of several ssDNA concentrations bound to the morpholino probe, achieving a sensitivity of 2.12 nm/nM with indicated standard deviation error bars obtained through repetitive scans of the same measurement; (b) Bar chart illustrating the wavelength shifts of four different ssDNA concentrations hybridized to the morpholino monolayer. Each hybridization experiment was conducted for a duration of 30 minutes.

TABLE II
COMPARISON OF PERFORMANCE METRICS BASED ON DIFFERENT TYPES OF BIOSENSORS DETECTING DNA HYBRIDIZATION
(ALL DETECTION LIMITS ARE DEFINED AS THE LOWEST CONCENTRATION TESTED)

Sensor design configuration	Capture probe - target analyte	DNA hybridization sensitivity (S_{DNA})	Detection limit	Intrinsic limit of detection (iLOD)
Fluorescence-based sensor				
Fluorescence microscopy [7]	MO - DNA	-	1 nM	-
Silicon nanowire sensor				
Si nanowire biosensor [10]	MO - DNA	-	100 fM	-
Electrochemical sensor				
Gold supports that monitor changes in interfacial capacitance [8]	MO - DNA	-	25 nM	-
Photonic sensor				
Porous Si ring resonator [41]	DNA - PNA	4 pm/nM	500 nM	42 nM
Suspended 90 nm slab micro-ring resonator (this work)	**MO - DNA**	**2.12 nm/nM**	**250 pM**	**36.9 pM**

was approximately $S_{\mathrm{DNA}} = 2.12$ nm/nM for the hybridization of ssDNA molecules.

In order to estimate the thickness of the surface layers, the simulated surface sensitivity obtained in Section II was combined with the experimental resonant wavelength shift of the 90 nm slab micro-ring resonator achieved in the bio-sensing demonstration. The surface sensitivity of the simulated device was 215.6 pm/nm for the first 20 nm-thick surface layer. Therefore, the surface layer thickness can be estimated ($\Delta t = \Delta\lambda / S_s$). For a total recorded resonant wavelength shift of: 1) 1.058 nm for APTMS; 2) 490.6 pm for glutaraldehyde; and 3) 93.7 pm for morpholino as shown in Fig. 6, the corresponding thicknesses of these deposited layers are: 1) 4.908 nm of deposited APTMS; 2) 2.276 nm of deposited glutaraldehyde; and 3) 0.434 nm deposited film of morpholino probe. For the largest DNA concentration tested (1 nM), the equivalent thickness of a resonant wavelength shift of ~2.35 nm is about ~10.9 nm. Therefore, the assumed total film thickness of the bound species up till hybridized DNA of the highest concentration was about ~18.5 nm, comparable to previously made assumptions [30].

To compare the limit of detection (LOD) of this work with published data, papers that report their LOD as the lowest DNA concentration tested were mentioned in this work. The LOD is quantified to be at least 3 times higher than the standard deviation of the noise floor level (3σ). In addition to the limit of detection, the intrinsic limit of detection ($i\mathrm{LOD} = \lambda_{\mathrm{res}}/(\tilde{Q} \times \tilde{S}_{\mathrm{DNA}})$) is also quantified for a photonic micro-ring resonator, to impartially compare sensor performance away from the influence of the readout equipment and the experimental setup. The lowest ssDNA concentration tested using the suspended 90 nm slab micro-ring resonator was 250 pM. The quantified iLOD in detecting morpholino-ssDNA hybridization for a λ_{res} of 1553.34 nm, and a Q of 19 840 was 36.9 pM.

In comparison to the silicon nanowire (SiNW) sensor that also used morpholino as a capture probe, as shown in Table II, its reported detection limit is smaller by 3 orders of magnitude

compared to the results of this work. Despite its high detection sensitivity, SiNWs have issues such as low reproducibility and low-throughput fabrication methods, in addition to the native oxide surface that acts as a dielectric, screening the nanowire from the analyte to be sensed [42]. On the other hand, photonic ring resonators enjoy advantages such as their scalable production and ease of integration with lab-on-a-chip techniques. In terms of detection performance, the 90 nm slab micro-ring resonator sensor demonstrated an LOD, that is 4 times and a 100 times smaller than the DNA concentration detected with the fluorescence-based sensor [7], and the electrochemical sensor [8], respectively. In comparison to the porous Si photonic ring resonator reported in [41], the 90 nm slab micro-ring resonator functionalized with the neutral morpholino probe exhibited a hybridization sensitivity that is 500-folds greater, and a detection limit smaller by 3 orders of magnitude.

It should be noted that the capture probe density and ionic strength have not been considered in the above comparisons. Contrasting different types of DNA detecting sensors and their design configurations is challenging because of several influencing variables (e.g. surface functionalization steps, testing conditions, and ionic buffer strength) that have an impact on the overall detection sensitivity. However, the comparison made in this work gives an indication of how the 90 nm slab micro-ring resonator performs against other sensors in its DNA detection.

As for the hybridization time, regardless of the DNA concentration tested, the 90 nm slab micro-ring resonator demonstrated successful hybridization within the same time frame ($\sim$18 minutes) although measurements were conducted after a 30-minute time lapse. In comparing the detection speed, a one-to-one comparison can be made with the fluorescence-based sensor [7] that shares similar experimental conditions (same morpholino probe) in observing its 1 nM DNA detection limit. This work demonstrated a detection speed increase by 32-folds when compared to the 16-hour time frame observed by the fluorescence-based sensor. This is partly due to the higher sensitivity, as well as the higher surface area enabled by the suspended structure. Therefore, the sensing scheme using the suspended micro-ring resonator, facilitated label-free detection and demonstrated an enhancement in the speed of detection with increased sensitivity, based on shorter diffusion length and larger surface area for molecular interaction.

V. Conclusion

In this study, the detection of morpholino-DNA hybridization has been investigated for the first time using a photonic suspended 90 nm slab micro-ring resonator. Several of the shortcomings that morpholino shares with conventional probes such as long hybridization time and poor sensitivity, especially with detecting low analyte concentrations, have been addressed in this work.

A sensitivity of 2.12 nm/nM and a LOD of 250 pM was achieved in detecting MO-DNA hybridization within $\sim$18 minutes. Characterization of the 90 nm slab ring also demonstrated a bulk refractive index sensitivity of $\sim$ 97.48 nm/RIU and an iLOD of $\sim 1 \times 10^{-3}$ RIU upon testing varying concentrations of isopropanol and deionized water.

Exploiting the benefits of a neutral-charged probe such as morpholino and a suspended resonant structure, the 90 nm slab ring sensor demonstrated an enhanced sensitivity, detection limit, and detection speed. Furthermore, the detection was label-free with no prior amplification process required for hybridization, all within a compact device footprint of 5.57 μm^2 modal effective area. Hence, the 90 nm slab micro-ring resonator proved as a promising candidate for future real bio-sensing applications.

References

[1] P.-E. Fournier, M. Drancourt, P. Colson, J.-M. Rolain, B. La Scola, and D. Raoult, "Modern clinical microbiology: New challenges and solutions," *Nature Rev. Microbiol.*, vol. 11, no. 8, pp. 574–585, 2013.

[2] T. R. Gingeras, R. Higuchi, L. J. Kricka, Y. D. Lo, and C. T. Wittwer, "Fifty years of molecular (DNA/RNA) diagnostics," *Clin. Chem.*, vol. 51, no. 3, pp. 661–671, 2005.

[3] C. Bedin, M. V. Enzo, P. Del Bianco, S. Pucciarelli, D. Nitti, and M. Agostini, "Diagnostic and prognostic role of cell-free DNA testing for colorectal cancer patients," *Int. J. Cancer*, vol. 140, no. 8, pp. 1888–1898, 2017.

[4] J.-S. Lee, M. S. Han, and C. A. Mirkin, "Colorimetric detection of mercuric ion (Hg^{2+}) in aqueous media using DNA-functionalized gold nanoparticles," *Angewandte Chemie Int. Ed.*, vol. 46, no. 22, pp. 4093–4096, 2007.

[5] Y.-T. Lo and P.-C. Shaw, "DNA-based techniques for authentication of processed food and food supplements," *Food Chem.*, vol. 240, pp. 767–774, 2018.

[6] Z. Gao and B. P. Ting, "A DNA biosensor based on a morpholino oligomer coated indium-tin oxide electrode and a cationic redox polymer," *Analyst*, vol. 134, no. 5, pp. 952–957, 2009.

[7] D. Martins, R. Levicky, and Y.-A. Song, "Enhancing the speed of morpholino-DNA biosensor by electrokinetic concentration of DNA in a microfluidic chip," *Biosensors Bioelectron.*, vol. 72, pp. 87–94, 2015.

[8] N. Tercero, K. Wang, P. Gong, and R. Levicky, "Morpholino monolayers: Preparation and label-free DNA analysis by surface hybridization," *J. Amer. Chem. Soc.*, vol. 131, no. 13, pp. 4953–4961, 2009.

[9] W. Hu, Q. Hu, L. Li, J. Kong, and X. Zhang, "Detection of sequence-specific DNA with a morpholino-functionalized silicon chip," *Anal. Methods*, vol. 7, no. 6, pp. 2406–2412, 2015.

[10] G.-J. Zhang, Z. H. H. Luo, M. J. Huang, G. K. I. Tay, and E.-J. A. Lim, "Morpholino-functionalized silicon nanowire biosensor for sequence-specific label-free detection of DNA," *Biosensors Bioelectron.*, vol. 25, no. 11, pp. 2447–2453, 2010.

[11] J. E. Summerton, "Morpholinos and PNAs compared," in *Peptide Nucleic Acids, Morpholinos and Related Antisense Biomolecules*. Berlin, Germany: Springer, 2006, pp. 89–113.

[12] C. S. Huertas, O. Calvo Lozano, A. Mitchell, and L. M. Lechuga, "Advanced evanescent-wave optical biosensors for the detection of nucleic acids: An analytic perspective," *Front. Chem.*, vol. 7, 2019, Art. no. 724.

[13] X. Tu, S.-L. Chen, C. Song, T. Huang, and L. J. Guo, "Ultrahigh Q polymer microring resonators for biosensing applications," *IEEE Photon. J.*, vol. 11, no. 2, Apr. 2019, Art. no. 4200110.

[14] J. D. Orlet and R. C. Bailey, "Silicon photonic microring resonator arrays as a universal detector for capillary electrophoresis," *Anal. Chem.*, vol. 92, no. 2, pp. 2331–2338, 2019.

[15] F. Vollmer and S. Arnold, "Whispering-gallery-mode biosensing: Label-free detection down to single molecules," *Nature Methods*, vol. 5, no. 7, pp. 591–596, 2008.

[16] F. Khozeymeh and M. Razaghi, "Characteristics optimization in single and dual coupled silicon-on-insulator ring (disk) photonic biosensors," *Sensors Actuators B: Chem.*, vol. 281, pp. 998–1008, 2019.

[17] H. Zhang, P. Palit, Y. Liu, S. Vaziri, and Y. Sun, "Reconfigurable integrated optofluidic droplet laser arrays," *ACS Appl. Mater. Interfaces*, vol. 12, no. 24, pp. 26936–26942, 2020.

[18] Z. Wang *et al.*, "Bio-electrostatic sensitive droplet lasers for molecular detection," *Nanoscale Adv.*, vol. 2, no. 7, pp. 2713–2719, 2020.

[19] E. Luan *et al.*, "Enhanced sensitivity of subwavelength multibox waveguide microring resonator label-free biosensors," *IEEE J. Sel. Topics Quantum Electron.*, vol. 25, no. 3, pp. 1–11, May/Jun. 2019.
[20] S. M. Lo, S. Hu, G. Gaur, Y. Kostoulas, S. M. Weiss, and P. M. Fauchet, "Photonic crystal microring resonator for label-free biosensing," *Opt. Exp.*, vol. 25, no. 6, pp. 7046–7054, 2017.
[21] V. Passaro, F. Dell'Olio, and F. De Leonardis, "Ammonia optical sensing by microring resonators," *Sensors*, vol. 7, no. 11, pp. 2741–2749, 2007.
[22] F. Dell'Olio, D. Conteduca, C. Ciminelli, and M. N. Armenise, "New ultrasensitive resonant photonic platform for label-free biosensing," *Opt. Exp.*, vol. 23, no. 22, pp. 28 593–28604, 2015.
[23] M. S. Murib, D. Martens, and P. Bienstman, "Label-free real-time optical monitoring of DNA hybridization using SiN Mach-Zehnder interferometer-based integrated biosensing platform," *J. Biomed. Opt.*, vol. 23, no. 12, 2018, Art. no. 127002.
[24] A. Liu, H. Huang, L. Chin, Y. Yu, and X. Li, "Label-free detection with micro optical fluidic systems (MOFS): A review," *Anal. Bioanalytical Chem.*, vol. 391, no. 7, pp. 2443–2452, 2008.
[25] C.-Y. Chao and L. J. Guo, "Design and optimization of microring resonators in biochemical sensing applications," *J. Lightw. Technol.*, vol. 24, no. 3, pp. 1395–1402, 2006.
[26] W. C. Jiang, J. Zhang, and Q. Lin, "Compact suspended silicon microring resonators with ultrahigh quality," *Opt. Exp.*, vol. 22, no. 1, pp. 1187–1192, 2014.
[27] M. F. O. Hameed and S. Obayya, *Computational Photonic Sensors*. Berlin, Germany: Springer, 2019.
[28] Y. Xiao *et al.*, "Towards integrated resonant and interferometric sensors in polymer films," *Procedia Technol.*, vol. 15, pp. 691–701, 2014.
[29] H. Yan *et al.*, "Unique surface sensing property and enhanced sensitivity in microring resonator biosensors based on subwavelength grating waveguides," *Opt. Exp*, vol. 24, no. 26, pp. 29724–29733, 2016.
[30] J. Flueckiger, "Enhancing the performance of silicon photonics biosensors," Ph.D. dissertation, Fac. Appl. Sci., Univ. Brit. Columbia, Canada, 2017.
[31] E. Luan, H. Shoman, D. M. Ratner, K. C. Cheung, and L. Chrostowski, "Silicon photonic biosensors using label-free detection," *Sensors*, vol. 18, no. 10, pp. 3519–3560, Oct. 2018.
[32] K. De Vos, "Label-free silicon photonics biosensor platform with microring resonators." Ph.D. dissertation, Dept. Inf. Technol., Ghent Univ., Ghent, Belgium, 2010.
[33] S. Schmidt, "Enhancing the performance of silicon photonic biosensors for clinical applications," Ph.D. dissertation, Dept. Bioeng., Univ. Washington, Seattle/Washington, USA, 2016.
[34] S. B. Nimse, K. Song, M. D. Sonawane, D. R. Sayyed, and T. Kim, "Immobilization techniques for microarray: Challenges and applications," *Sensors*, vol. 14, no. 12, pp. 22208–22229, 2014.
[35] S. T. Fard *et al.* "Performance of ultra-thin SOI-based resonators for sensing applications," *Opt. Exp.*, vol. 22, no. 12, pp. 14166–14179, 2014.
[36] G. Abbate, U. Bernini, E. Ragozzino, and F. Somma, "The temperature dependence of the refractive index of water," *J. Phys. D: Appl. Phys.*, vol. 11, no. 8, pp. 1798–1799, 1978.
[37] G. M. Hale and M. R. Querry, "Optical constants of water in the 200-nm to 200-μm wavelength region," *Appl. Opt.*, vol. 12, no. 3, pp. 555–563, 1973.
[38] S. TalebiFard *et al.*, "Optimized sensitivity of silicon-on-insulator (SOI) strip waveguide resonator sensor," *Biomed. Opt. Exp.*, vol. 8, no. 2, pp. 500–511, 2017.
[39] S. Schmidt *et al.* "Improving the performance of silicon photonic rings, disks, and Bragg gratings for use in label-free biosensing," in *Proc. SPIE*, vol. 9166, 2014, Art. no. 91660M.
[40] P. Liu and Y. Shi, "Simultaneous measurement of refractive index and temperature using a dual polarization ring," *Appl. Opt.*, vol. 55, no. 13, pp. 3537–3541, 2016.
[41] G. A. Rodriguez, S. Hu, and S. M. Weiss, "Porous silicon ring resonator for compact, high sensitivity biosensing applications," *Opt. Exp.*, vol. 23, no. 6, pp. 7111–7119, 2015.
[42] Y. L. Bunimovich, Y. S. Shin, W.-S. Yeo, M. Amori, G. Kwong, and J. R. Heath, "Quantitative real-time measurements of DNA hybridization with alkylated nonoxidized silicon nanowires in electrolyte solution," *J. Amer. Chem. Soc.*, vol. 128, no. 50, pp. 16323–16331, 2006.